Plasticity of the xylem vulnerability to embolism in Populus tremula x alba relies on pit quantity properties rather than on pit structure

Cedric Lemaire, Nicole Brunel-Michac, Jérémie Santini, Liliane Berti, Julien Cartailler, Pierre Conchon, Eric Badel, Stéphane Herbette

1   **Research Paper**

2   **Plasticity of the xylem vulnerability to embolism in *Populus tremula* x *alba* relies on pit**

3   **quantity properties rather than on pit structure**.

4   Cédric Lemaire [1], Yann Quilichini [2], Nicole Brunel-Michac [1], Jérémie Santini [2], Liliane Berti [2],

5   Julien Cartailler [1], Pierre Conchon [1], Éric Badel [1] and Stéphane Herbette [1].

6   [1] Université Clermont Auvergne, INRAE, PIAF, F-63000 Clermont-Ferrand, France.

7   [2] UMR 6134 SPE, CNRS-Università di Corsica, 20250 Corti, France

8

9   **Keywords**

10   Acclimation, anatomy, cavitation, hydraulic, phenotypic plasticity, Poplar, shade, water stress,

11   X-ray microCT.

12

13   **Running head**

14   Structural determinants of plasticity of embolism resistance

15

16   **Full address of the corresponding author**

17   Stéphane Herbette

18   UMR INRAE/UCA 547 PIAF

19   Université Clermont Auvergne, Campus Universitaire des Cézeaux,

20   1 Impasse Amélie Murat,

21   TSA 60026, 63178 AUBIERE Cedex

22   FRANCE

23   Stephane.Herbette@uca.fr

1

24   **Abstract**

25   Knowledge on variations of drought resistance traits are needed to predict the potential of trees

26   to acclimate to coming severe drought events. Xylem vulnerability to embolism is a key

27   parameter related to such droughts, and its phenotypic variability relies mainly on

28   environmental plasticity. We investigated the structural determinants controlling the plasticity

29   of vulnerability to embolism, focusing on the key elements involved in the air bubble entry in

30   vessels, especially the inter-vessel pits. Poplar saplings (*Populus tremula x alba*) grown in

31   contrasted water availability or light exposure exhibited differences in vulnerability to

32   embolism (P_{50}) in a range of 0.76 MPa. We then characterized the structural changes in features

33   related to pit quantity and pit structure, from the pit ultrastructure to the organization of xylem

34   vessels, using different microscopy techniques (TEM, SEM, LM). A multispectral combination

35   of X-ray microtomography and light microscopy analysis allowed measuring the vulnerability

36   of each single vessel and testing some of the relationships between structural traits and

37   vulnerability to embolism inside the xylem. The pit ultrastructure did not change, whereas the

38   vessel dimensions increased with vulnerability to embolism and the grouping index and fraction

39   of inter-vessel cell wall both decreased with vulnerability to embolism. These findings hold

40   when comparing between trees, or between the vessels inside the xylem of an individual tree.

41   These results evidenced that plasticity of vulnerability to embolism in hybrid poplar occurs

42   through changes in the pit quantity properties such as pit area and vessel grouping rather than

43   on the pit structure.

44   **Keywords**

45   Acclimation, anatomy, cavitation, hydraulic, phenotypic plasticity, Poplar, shade, water stress,

46   X-ray microCT.

47

Introduction

According to the cohesion-tension theory (Steudle 2001), the water columns in the xylem are under tension, a metastable state. When this tension increases during droughts, the water columns are more prone to break, because of cavitation: vapour bubbles invade the impacted vessels and spread, impeding function and leading to a loss of xylem conductance. When the loss of conductance reaches a threshold (around 90%), the distal organs are not supplied with water anymore leading to death (Barigah et al. 2013). For woody species, drought-induced death is more likely due to xylem hydraulic failure (Anderegg et al. 2015, 2016, Adams et al. 2017) caused by embolism in the xylem conduits, even if other processes can also contribute to this death (Hammond et al. 2019) such as the carbon starvation (Hartmann et al. 2015).

A global analysis pointed out the narrow hydraulic safety margin at which woody species usually operate (Choat et al. 2012); inferring that research is needed on the variability of vulnerability to embolism. Within-species variability for vulnerability to embolism was shown for many tree species (e.g. Martínez-Vilalta et al. 2009, Herbette et al. 2010). The genetic variability for this trait is rather limited in both natural populations (Lamy et al. 2011, Wortemann et al. 2011) and cultivated species (Jinagool et al. 2015, 2018). This trait would be genetically canalized (Lamy et al. 2012) and varies mainly via plasticity due to environmental factors (Herbette et al. 2010). Plasticity of vulnerability to embolism was reported mainly under water stress, with wood formed under drier conditions being less vulnerable (Awad et al. 2010, Fichot et al. 2010, Plavcová and Hacke 2012). Other conditions such as shade or fertilization were associated to an increase in vulnerability to embolism (Cooke et al. 2005, Barigah et al. 2006, Plavcová and Hacke 2012). However, information is scarce on the determinants of plasticity of vulnerability to embolism. The structural determinants need to be deciphered first, before searching for their genetic control, as it can be complex to decipher the role of candidate genes (Allario et al. 2018).

73   In angiosperms, water flows between xylem vessels through bordered pits. These pits are

74   openings in the secondary cell wall that allow water to flow between vessels while they prevent

75   air seeding from neighbouring air-filled vessels. Pits have been identified as the key structures

76   for vulnerability to embolism (Lens et al. 2013; Jansen et al. 2018, Kaack et al. 2019). Thus,

77   we assume that the acclimation of vulnerability to embolism to environmental conditions would

78   involve changes in the pit quantity and/or structure, i.e. at pit and/or vessel scales (Lens et al.

79   2013). The key role of the pit ultrastructure in vulnerability to embolism has been evidenced in

80   several studies (e.g. Choat et al. 2008, Lens et al. 2011, Tixier et al. 2014), especially the pit

81   membrane (Jansen et al. 2009, Li et al. 2016, Kaack et al. 2019). There is a well-established

82   correlation between pit membrane thickness and vessel resistance to embolism in angiosperms

83   (Lens et al. 2011, Plavcová and Hacke 2012, Scholz et al. 2013a, Schuldt et al. 2016). A

84   mechanistic explanation has been provided through the recent discoveries on the three-

85   dimensional structure of the pit membrane (Kaack et al. 2019, 2020). Pit membrane is a porous

86   medium with series of various pore constrictions influencing the air seeding, and constriction

87   sizes decreased with increasing pit membrane thickness. Vulnerability to embolism is also

88   dependent on pit quantity parameters such as the pit area or the vessel connectivity and thus on

89   vessel dimensions and three dimensional organization (Lens et al. 2013). Zimmermann and Jeje

90   (1981) already pointed out that the hydraulic vulnerability could be related to the vessel volume

91   that varies depending on both their diameter (Tyree et al. 1994) and their length (Scholz et al.

92   2013a). Several studies demonstrated a relationship between vulnerability to embolism and

93   vessel diameter (Wheeler et al. 2005, Hacke et al. 2006, Maherali et al., 2006; Awad et al. 2010,

94   Hajek et al., 2014). However, other studies failed to detect such a relationship (Lens et al., 2011,

95   Scholtz et al. 2013 a, Schuldt et al. 2016). Such discrepancy between findings can be explained

96   by uncertainties about the relationship between vessel diameter and pit area. More, one has to

97   acknowledge that vulnerability to embolism is not controlled exclusively by either pit quantity

98   parameters or pit structure (Choat and Pittermann 2009). The three-dimensional organization

99   of the xylem network would also influence the vulnerability to embolism, as shown in

100   theoretical and empirical analyses (Loepfe et al. 2007, Mrad et al. 2018). The relationship

101   between vulnerability to embolism and pit properties has been intensively studied at the inter-

102   specific level, whereas the determinants of plasticity of vulnerability to embolism remain poorly

103   investigated at the intraspecific level (Schuldt et al. 2016). For example, in poplar, Plavcová et

104   al. (2011) showed that shading caused an increase in vulnerability to embolism associated with

105   a decrease in both pit membrane thickness and vessel diameter, whereas Awad et al. 2010

106   showed that a reduced watering induced a decrease in vulnerability to embolism linked with a

107   decrease in vessel diameter.

108   In this work, we investigated the relationship between the plasticity of vulnerability to

109   embolism and changes in structures related to pit properties at different anatomical levels on

110   young poplars (*Populus tremula x alba*). We grew saplings of a poplar clone under three

111   contrasted environmental conditions for two factors (water and light availability) known to

112   induce variation of vulnerability to embolism. Then, their xylem anatomy was analysed in

113   relation to the changes in vulnerability to embolism using different approaches. Transmission

114   Electron Microscopy (TEM) allowed investigations on the pit ultrastructure. Parameters related

115   to the pit-field were measured using Scanning Electron Microscopy (SEM). We also measured

116   pit quantity parameters related to vessel dimensions and vessel connectivity using light

117   microscopy and silicon injections. Then, an approach using direct observation of embolism

118   spreading inside the xylem by X-ray microtomography allowed to analyse the relationships

119   between structural traits and vulnerability to embolism at the vessel level.

120

121   **Materials and Methods**

122   **Plant material and growth conditions**

123   *Plant Material.* Saplings of hybrid poplar (*Populus tremula x alba* clone INRA 717-1B4) were

124   propagated clonally *in vitro* on Murashige and Skoog medium on December 2016. Plantlets

125   were transferred in hydroponic solution on February 2017 and grown in a controlled

126   environment room: 16 h daylight at 21-22 °C, 40 $\mu mol.m^{-2}.s^{-1}$ and 18-19 °C night, at 70 ± 10 %

127   relative humidity. On March 2017, plants were transferred in 1 Litre pots filled with potting

128   soil (Humustar Terreaux, Champeix, France) with a composition of 25 % brown peat, 40 %

129   blond peat and 35 % pine bark dust. The pots were placed in a greenhouse at the INRAE

130   research station of Clermont-Ferrand, France (site of Crouël; N 45°77′, E 3°14′; 300 m *a.s.l.*).

131   After 20 days, plants were transferred in 10 L pots filled with potting soil. They were regularly

132   watered at soil field capacity. Each pot weighted 6.4 ± 0.4 kg. Ten days later, the specific

133   experimental growth conditions were applied (see next). After one month of growth, stems were

134   cut at 50 cm height. The growth of a new apical bud occurred in May 2017, and any additional

135   bud was removed. Thus, a single stem completely grew under the new environmental

136   conditions.

137   *Experimental setup.* Plants were split in three groups submitted to different growth conditions:

138   (i) "control" plants grew under full sunlight and watered at soil field capacity; (ii) "droughted"

139   plants grew under full sunlight and watered at 25-30 % of soil field capacity; (iii) "shaded"

140   plants shaded by a shadehouse that intercepted 30 % of incident light and watered at soil field

141   capacity. For the nine droughted plants, an irrigation at 25-30 % of soil field capacity was kept

142   constant in each pot individually using balances and automatic valves for irrigation as described

143   in Niez et al. (2019). We measured the light interception by the shadehouse by comparing for

144   two months the light intensities recorded with two sensors (PAR/CBE 80, Solems, Palaiseau,

145   France) placed inside the shadehouse and two sensors placed outside. The level of water stress

146   was set to be the most restrictive while allowing growth to produce acclimatized xylem and

147   enough plant material for further analyses. The stem diameter was continuously measured using

6

148   a LVDT sensor (Linear Variable Differential Transformer) on three droughted, two control and

149   three shaded plants. Plant height was measured using a measuring tape.

150   One month before and the day before the tree sampling, predawn water potential (Ψ_{pd}) was

151   measured on every plant 1 hour before the sunrise using a pressure chamber (1505D, PMS

152   Instrument, Albany, OR, USA, Scholender et al. 1965). The same day, midday water potential

153   (Ψ_{mid}) was measured at the solar noon, between 12:00 and 2:00 PM.

154   *Sampling protocol.* The sampling was performed on 28 August 2017. Plants were cut at 20 cm

155   height. The plant shoot was immerged underwater and the 30 cm of the top were removed as it

156   lacks significant secondary xylem. Then, the following stem segments were sampled, from

157   basal to apical direction:

158   i) the 30 cm long basal part of the stem was removed because it was not fully grown under

159   acclimation conditions;

160   ii) the first 50 cm long of the newly developed stem under the acclimation conditions was

161   wrapped in wet paper, put in a plastic bag and stored at 4 °C until measurements of vulnerability

162   to embolism and vessel length;

163   iii) the above segment of 6 cm long was devoted to microscopy analyses. It was split into three

164   subsamples using a razor blade: two segments of 1 cm long were prepared for light microscopy

165   and TEM observations. A third segment of 4 cm long was prepared for SEM observations;

166   iv) if the stem was long enough, an additional segment of 50 cm long was wrapped in wet paper

167   in a plastic bag, and stored at 4 °C for measurements of specific conductivity (K_S) and for

168   additional measurements of vulnerability to embolism;

169   v) the last 10 cm long was kept wrapped in humid paper for a native embolism measurement

170   performed on the sampling day.

171   Leaves were sampled under water and the total leaf area (LA) per plant was measured in the

172   day using an area-meter (Li-3100c, Li-Cor Biosciences, Lincoln, NE, USA).

173   After the sampling, plants were kept in the greenhouse, during the winter 2017. On March 2018,

174   they started growing, still under the same environmental conditions as described above, and on

175   July 2018 we performed a second sample collection: plants were cut at 25 cm height. Then the

176   30 cm long basal part of the stem was cut underwater. A 50 cm long sample was wrapped in

177   wet paper and stored in a plastic bag at 4 °C for measurements of specific conductivity (K_S).

178   **Hydraulic traits measurements:**

179   *Vulnerability to embolism.* The 50 cm long stem segment was shortened underwater at 43 cm

180   long using a razor blade. Then, the vulnerability to embolism was assessed using the Cavitron

181   technique (Cochard 2002, Cochard et al. 2005). A centrifugal force increases water tension in

182   branch segment while a specific optical device allows the continuous measurement of the loss

183   of conductance (Cochard et al. 2009). A vulnerability curve was built by plotting the percentage

184   loss xylem conductance (PLC) *vs.* xylem water pressure (*P*). A sigmoidal function was used to

185   fit each curve using the equation 1 (Pammenter and Willigen 1998).

186
$$\text{PLC} = \frac{100}{1 + e^{\frac{S\,(P - P_{50})}{25}}} \qquad\qquad (1)$$

187   Where P_{50} is the pressure causing 50 % loss of conductance, and *S* is the slope of the curve at

188   this point.

189   *Specific conductivity.* Stem segments of 50 cm long were shortened underwater at a length

190   (L_{stem}) of 40 cm long using a razor blade for droughted (n = 8), control (n = 9) and shaded (n =

191   9) plants. The apical end of the sample was sealed to a tubing system (polytetrafluoroethylene

192   film) and plugged to an embolism meter (Xyl'em, Bronkhorst, Montigny les Cormeilles,

193   France). The initial conductance (K_i) was then measured under low pressure (2 to 7 kPa) using

194   a solution of 10 mM KCl and 1 mM $CaCl_2$. The xylem area A_X of the distal end of the sample

195   was measured on a cross section using a scanner (V800, Epson, Nagano, Japan). The

196   measurement of A_x was performed on the scanned image using the ImageJ software (version

197   v.1.52c) (Schneider et al. 2012). The Specific Conductivity K_S was defined according to

198   equation 2.

199   $$K_S = \frac{K_i \times L_{stem}}{A_x} \qquad (2)$$

200   *Native Embolism.* The native embolism of the stem segments of 10 cm long were measured on

201   the sampling day for droughted (n = 9), control (n = 5) and shaded (n = 6) plants. Each sample

202   was shortened underwater using a razor blade to a length of 8 cm. Then, the initial conductance

203   (K_i) was measured under low pressure (2 to 7 kPa) with the same method and the same solution

204   as for specific conductivity. Then, the sample was flushed with the same solution twice for

205   5 min under high pressure (0.1 to 0.2 MPa) in order to remove the air embolism. A new

206   measurement of conductance without embolism indicated the maximum conductance (K_{max}) of

207   the sample. The native embolism was calculated according to the equation 3.

208   $$\text{Native Embolism} = (1 - \frac{K_i}{K_{max}}) \times 100 \qquad (3)$$

209   **Light microscopy**

210   Samples of 1 cm long were cut into 3 x 3 mm² blocks then they were immersed in Karnvosky's

211   fixative solution under vacuum for 30 min, then stored at 4 °C in the fixative solution up to the

212   next step. Then, they were dehydrated in an ethanol series (50, 70, 80, and 95 %) and embedded

213   in LR White resin. Transverse slices of 2 to 3 µm thick were cut using an ultramicrotome (Om

214   U2, Reichert, Vienna, Austria). Sections were stained with 1 % (w/v) toluidine blue, washed 4

215   times with water and mounted in Eukitt (Sigma-Alrich, St-Louis, MO, USA). Images were

216   processed using a microscope (Zeiss Axio Observer Z1), a digital camera (AxioCam MRc) and

217   Zen imaging software system (Zeiss, Jena, Germany).

218   Image analyses were performed using ImageJ software with a home-made semi-automated

219   procedure. The vessel diameter (D_v) was estimated to be the diameter of the circle having the

220   same area as the vessel lumen (for the symbols, see Table 1). The total vessel wall perimeter in

221   contact with other vessel was measured using the Feret diameters. The vessel diameters were

222   increased by five pixels using dilate function and if dilated vessels overlapped, they were

223   considered to be in contact. The maximum Feret diameter of the overlapping area was

224   considered to be their length of wall in contact. From there, the contact fraction (F_c) was

225   measured for each vessel as the ratio of length of wall in contact with other vessels over the

226   perimeter of the vessel. Vessels that shared wall were assigned to the same group. As a result,

227   the two-dimensional grouping index (GI) was the mean number of vessels per group and the

228   solitary index (SI) as the ratio of the number of solitary vessels to the total number of vessels.

229   These parameters were measured for each individual slice containing a mean of 850 vessels,

230   for droughted (n = 9), control (n = 5) and shaded (n = 6) plants.

231   **Vessel length**

232   The vessel length was measured by the silicon injection method (Sperry et al. 2005, Scholz et

233   al. 2013b) on the samples already used for Cavitron technique, after five months of drying at

234   room temperature. A fluorescent optical brightener (CAS number: 7128-64-5, Sigma-Aldrich,

235   St-Louis, MO, USA) was mixed in chloroform (1 % w/w) and added to a volume of silicon

236   (BLUESIL RTV-141 A, Bluestar Silicones, Lyon, France) with a proportion of one drop of

237   solution per gram of silicon. A Silicone hardener (BLUESIL RTV-141 B, Bluestar Silicones)

238   was added to the mixture in 1:10 proportion. The mixture was then injected under pressure (300

239   to 400 kPa) basipetally in the stem sample using a pressure chamber during at least 8 hours.

240   After silicone hardening (3 days at room temperature), the samples were cut 5 mm far from the

241   injection point; then every 20 mm. For each segment, a 25 µm thick slice was cut using a rotary

242   microtome (RM2165, Leica Microsystems, Wetzlar, Germany). Cross sections were dyed with

243   Astra Blue and mounted with a glycerol medium.

244   Images were obtained using a fluorescence microscope (Axio Observer Z1) equipped with a

245   300 to 400 nm band pass excitation filter, a digital camera (AxioCam 506), Zen imaging

246   software system (Zeiss, Jena, Germany) and analysed using the ImageJ software. Fluorescent

247 vessels highlighted the open vessels, while white light allowed counting the total number of

248 vessels. The decrease of the ratio of open vessels (N_x) (*i.e.* fluorescent vessels) to the total

249 number of vessels (N_0) over the distance (x) from the end of the sample followed an exponential

250 decay function (equation 4) where k is the best-fit extinction coefficient (Cohen et al. 2003).

251 $$N_x = N_0 \times e^{-kx} \qquad (4)$$

252 The fraction of conduits of length x ($P(x)$) is obtained by multiplying x/N_0 to the second

253 derivative of equation 4 (Wheeler et al. 2005):

254 $$P(x) = x \times k^2 \times e^{-kx} \qquad (5)$$

255 The continuous cumulative function of vessel length (Lv) probability is a function given in the

256 equation 6.

257 $$f(x) = \int_0^{L_v} x k^2 . e^{-kx} dx \qquad (6)$$

258 When this cumulative function is equal to 0.5, this gives the median value of vessel length

259 (L_v) (equation 7).

260 $$f(L_v) = -(kL_v + 1).e^{-kL_v} + 1 = 0.5 \qquad (7)$$

261 The solution of the equation 7 gives the median vessel length $L_v = 1.678/k$. This vessel

262 length was estimated for 7 droughted, 5 control and 5 shaded stem samples.

263 **Transmission Electron Microscopy**

264 Fresh samples of 1 cm long were cut into 2 to 4 mm^3 blocks, immersed in Karnvosky's fixative

265 solution under vacuum for 30 min, then stored at 4 °C in the fixative solution for 3 weeks.

266 Blocks were recut into 1 to 2 mm^3 pieces, then they were fixed secondarily for 4 hours at

267 ambient temperature in a 0.1M phosphate-buffered osmium tetroxide solution (1 %), pH 7.4.

268 Then, they were dehydrated in an ethanol series (25, 50, 70, 100, and 100 %) and embedded in

269 Epoxy resin using Epoxy medium kit (Sigma-Aldrich, St-Louis, MO, USA). Then, ultra-thin

270 sections (60-90 nm) were cut using an ultramicrotome (PowerTome PC, RMC Boeckeler,

271 Tucson, AZ, USA). The sections were placed on 200- and 300-mesh copper grids and stained

272   with contrast solutions: UranyLess (Delta Microscopies, Mauressac, France) and lead citrate.

273   Sections were observed using a transmission electron microscope (H-7650, Hitachi High-

274   Technologies Corporation, Tokyo, Japan) at a voltage of 80 kV. Measurements of pit features

275   were performed on images with pits showing two apertures. Pits were characterized for their

276   diameter (D_p), their aperture diameter (D_a), their chamber depth (L_p) and their membrane

277   thickness (T_m). For each pit, D_a was the mean of two measurements while L_p and T_m were the

278   mean of four measurements. Pit features were measured for five individual trees for each

279   growth condition, with at least 10 pits measured per individual tree.

280   **Scanning Electron Microscopy**

281   Fresh samples were fixed in 3 % glutaraldehyde and stored at 4 °C for at least 1 month. Samples

282   of 4 cm long were cut longitudinally and then dehydrated in an ethanol series (30, 50, 75, and

283   100 %). After dehydration, samples were immerged in a 1:1 solution hexamethyldisilazane

284   (HMDS) + ethanol 100 % for 30 min and immerged in pure HDMS for 30 min. After air drying

285   overnight under a hood, the samples were mounted on aluminium stubs with carbon double-

286   sided adhesive disks, coated with gold/palladium in a sputter coater (SC7640, Quorum

287   Technologies Ltd, Newhaven, U.K.), and finally observed using a scanning electron

288   microscope (S-3400N, Hitachi High-Technologies Corporation, Tokyo, Japan) at a voltage of

289   5 kV. The portion of area covered by bordered pits in each inter-vessel pit-field (F_{pf}) was then

290   measured by image analysis using the ImageJ software. Five samples were measured per growth

291   condition, and seven pit-fields were characterized per sample.

292   **Estimation of supplementary hydraulic and structural traits**

293   Theoretical conductivities (K_{s_theo}) of all samples characterized by light microscopy were

294   calculated according to Scholz et al. (2013b) and converted into g.s⁻¹.MPa⁻¹.m⁻¹ (equation 8).

295
$$K_{s\_theo} = \frac{\Sigma \frac{\pi D_v^4}{128 \eta}}{A_x} \times \rho \qquad (8)$$

296 Where η is the viscosity index of water (1.002×10^{-9} m^4.MPa^{-1}.s^{-1} at 20 °C), ρ is the density of

297 water (9.982×10^5 g.m^{-3}) and A_x is the xylem cross-section area.

298 The pit fraction (F_p) was defined as the product of the pit-field fraction (F_{pf}) and the contact

299 fraction (F_c) (equation 9).

300 $$F_p = F_{pf} \times F_c \qquad (9)$$

301 The pit fraction was measured on five individual trees for each growth condition.

302 The vessel area (A_v) was estimated as the area of a cylinder according to the equation 10.

303 $$A_v = D_v \times L_v \times \pi + 2\pi\left(\frac{D_v}{2}\right)^2 \qquad (10)$$

304 It was measured for 7 droughted, 5 control and 5 shaded trees.

305 The pit area per vessel (A_p) was calculated as the product of the vessel area A_v by pit fraction

306 F_p (equation 11).

307 $$A_p = A_v \times F_p \qquad (11)$$

308 It was measured for 4 droughted, 5 control and 4 shaded individuals.

309 Xylem water potentials at the onset of xylem embolism (P_{12}) and at full embolism (P_{88}) were

310 calculated using equation 12 and 13 respectively (Domec and Gartner 2001), using the

311 experimental values of P_{50} and S resulting from equation 1.

312 $$P_{12} = P_{50} + \frac{50}{S} \qquad (12)$$

313 $$P_{88} = P_{50} - \frac{50}{S} \qquad (13)$$

314

315 **Measurement of individual vessel vulnerability to embolism using multispectral approach**

316 **combining X-ray microtomography and light microscopy**

317 Two stem segments from droughted plants and two from control plants were sampled and

318 prepared in the same condition as for vulnerability to embolism measurements. We used the

319 techniques described in Cochard et al. (2015). Segments were shortened underwater at 34 cm

320   long using a razor blade, sealed in liquid paraffin wax in order to prevent dehydration during

321   the microtomography scans. A first 21 min scan was acquired using a X-ray microtomography

322   system (Phoenix Nanotom, General Electric, Boston, MA, USA) at the centre of the segment

323   as described below to reveal the native state of embolism in each shoot. The field-of view was

324   $7.8 \times 7.8 \times 7.8$ mm^3 and covered each full cross section of the samples. X-ray source settings

325   were 60 kV and 240 μA. 1000 images were recorded during the 360 ° rotation of the sample

326   and the final spatial resolution was 3.9 μm.

327   Then, the paraffin was broken at the ends in order to allow the water flow and the sample was

328   set in a Cavitron during 5 min at 0.8 MPa, immersed in paraffin and scanned again with the X-

329   ray microtomograph at the same location than previously in order to observe the new embolism

330   status. The same procedure was repeated for increasing pressure steps, until - 4 MPa (Fig. 1).

331   Then, the stem sample was cut in the air at 5 mm above the scanned section in order to generate

332   100 % of embolism of the functional vessels and a last microtomographic scan was performed

333   in order to visualize this complete vessel network.

334   The sample was then dried several days in room conditions and a transverse section of 25 μm

335   thick was cut with a rotary microtome (RM2165, Leica Microsystems). Sections were dyed

336   with series of baths as following: bleach (about 15 sec), acetic acid, Astra blue (1 min), acetic

337   acid, safranin (1 min), acetic acid with a water bath between each solution, then an ethanol

338   series (50, 70, 100 and 100 %). The sections were mounted in Eukitt. Images were processed

339   using a microscope (Zeiss Axio Observer Z1), a digital camera (AxioCam MRc) and Zen

340   imaging software system (Zeiss, Jena, Germany). Image analyses were performed using Fiji

341   software (under ImageJ version 2.0.0-rc-68/1.52h) (Schindelin et al. 2012, Schneider et al.

342   2012), using the same method described in the section for light microscopy. The diameter of

343   each vessel (D_v^*) was estimated as the diameter of the circle that provided the same area as the

344   vessel lumen. For each vessel, the number of vessels in the group (Group Size; GS) and the

345　　fraction of membrane in contact with other vessels (F_c^*) were also estimated on the cross-

346　　section plane. Finally, the relative distance from the pith was measured for each vessel as the

347　　ratio of the distance from the pith to the vessel over the distance from the pith to the cambium.

348　　The microtomography scans were reconstructed in three-dimension (3D) using Phoenix datosx

349　　2 software (General Electric, Boston, MA, USA) with spatial resolution of 6.8 × 6.8 × 6.8 μm^3

350　　per voxel. Then, for each 3D-reconstruction, a cross section was extracted at the exact same

351　　location as with the microscopy section. For each vessel in the cross sections, its embolism

352　　pressure (P_e) is defined as being the centrifugation-induced pressure from which the vessel

353　　appeared to be air-filled on microtomographic images (Fig. 1, A-D).

354　　For each sample, images from x-ray microtomography observation (virtual cross sections built

355　　by 3D reconstruction) were aligned on the light microscopy image (stem cross section observed

356　　by light microscopy) using the "Align image by line ROI" tool (Schindelin et al. 2012) of Fiji

357　　software. A unique identification number was given to each vessel observed in images from

358　　both techniques, in order to link the embolism pressure with anatomical parameters (Fig. 1, E).

359　　A total of 2570 vessels were identified. Vessels were grouped per D_v^*, per F_c^* and per GS

360　　classes. Classes were sized to be as uniform as possible, counting from 183 up to 748 vessels.

361　　A total of 1100 solitary vessels were grouped in the same class when required. Cumulative

362　　number of embolized vessels was plotted according to their P_e and, for each class, a Weibull

363　　function was fit (equation 1).

364　　**Statistical analysis**

365　　The statistical analysis was performed using the RStudio software (version 1.1.456; running

366　　under R core version 3.5.1, R Development Core Team 2008). One way ANOVA was used for

367　　comparing the means between the three growth conditions. When we found a significant

368　　difference, we referred to Tukey's multiple range test at $p < 0.05$ to compare the mean values

369   between growth conditions. The correlations between the structural traits and the P_{50} and P_e

370   were calculated using linear regressions.

371

372   **Results**

373   Continuous recordings of the radial growth showed a significant lower growth for the droughted

374   plants throughout the experiment (Fig. S2, Table 2). These plants also showed a lower height,

375   lower leaf area, lower Ψ_{pd} and lower Ψ_{md}, demonstrating the significant effect of our drought

376   treatment. The higher leaf area for shaded plants compared to control plants is an evidence that

377   the shading conditions affected the plant development.

378   Growing plants under different environmental conditions aimed to induce wide variations in

379   xylem vulnerability to embolism. The three growth conditions spread the measured P_{50} over

380   range from - 2.00 to - 3.47 MPa (Table S1), with a difference of 1.04 MPa between the most

381   resistant droughted plant and the most vulnerable control plant and a difference of 1.47 MPa

382   between the most resistant droughted plant and the most vulnerable shaded plant. A

383   significantly lower P_{50} was found on droughted plants when compared to control and shaded

384   plants (*p < 0.001*, Table 2), while the slopes of the vulnerability curves were not different

385   between the growth conditions (Fig. 2, A). Despite a slightly higher native embolism for

386   droughted plants compared to shaded plants, Ψ_{mid} was higher than the inflexion point of the

387   vulnerability curve (P_{12}) for every growth conditions. This allows excluding any effect of these

388   quite low native embolism on measured P_{50}. We observed no difference for mean K_S between

389   the growth conditions (Fig. 2, B), suggesting no plasticity for this trait in our experimental

390   conditions. When considering the vessel diameter, a reduced K_{s_theo} was measured in the

391   droughted plants compared to control and shaded plants (Table 2).

392   The analyses combining different methods (light microscopy, TEM, SEM), allowed measuring

393   a large set of anatomical traits from tissue to pit levels. The correlation between these traits and

394   the P_{50} was assessed (Fig. 3, 4).

395   The traits measured at tissue level (GI, SI and F_p) showed a strong linear correlation with P_{50}

396   ($R^2 > 0.70; p < 0.001$; Fig. 3, 4), except F_c that exhibited a weaker correlation ($R^2 = 0.38; p =$

397   0.004). These results put in light a relationship between vessel connectivity, vessel grouping

398   and vulnerability to embolism (negative relationship for F_c, GI and F_p; positive relationship for

399   SI). However, we found no correlation between pit-field fraction (F_{pf}) and P_{50}, with no variation

400   among the growth conditions (Table 3). We observed a strong positive relationship ($p < 0.001$)

401   between P_{50} and the vessel dimensions (L_v, D_v and A_v) showing that larger vessels with larger

402   pit area tend to be associated with an increase in vulnerability to embolism ($R^2 > 0.75;$

403    $p < 0.001$). The positive correlation between P_{50} and A_p ($R^2 = 0.78; p < 0.001$, Fig. 4)

404   highlighted the link between the area of vessels covered by bordered pits and the xylem

405   vulnerability to embolism.

406   No linear correlation appeared between the pit structure parameters (D_a, D_p, L_p and T_m) and the

407   P_{50}: we observed no variation for D_a, D_p and T_m among growth conditions.

408   Using x-ray microtomograph, the direct visualization of embolism inside the xylem (Fig. 1)

409   allowed evaluating the vulnerability to embolism (P_e) of individual vessels. The multispectral

410   analysis combining x-ray tomographic observations and the measurements made on light

411   microscopy images allowed establishing the link between P_e and the structural parameters of

412   each vessel (Fig. 5). The correlation between D_v^* and P_e (Fig. 5, A) was clear: wider vessels

413   appeared more vulnerable than the narrower ones. F_c^* showed a smaller influence on P_e (Fig.

414   5, B): solitary vessels ($F_c^* \leq 1$ %) and weakly connected vessels ($1 < F_c^* \leq 20$ %) were more

415   vulnerable than the highly connected vessels ($F_c^* > 20$ %). The link between GS and P_e (Fig. 5,

416   C) appeared to be the less clear: the most vulnerable vessels were the solitary ones whereas the

417 grouped vessels ($GS \geq 2$) were less vulnerable. Despite a significant correlation between P_e

418 and D_v^*, F_c^* and GS ($p < 0.001$; Fig. 6), the strength of the correlation was poor ($R^2 < 0.25$).

419 We also noticed that the position of the vessel in the cross section is linked to its vulnerability

420 (Fig 1): the more the vessels were far from the pith, the more they were more resistant to

421 embolism. ($R^2 = 0.49$; $p < 0.001$; Fig. 5, D; Fig. 6).

422

423 **Discussion**

424 The range for P_{50} plasticity induced by the growth conditions was large: 0.76 MPa between the

425 mean P_{50} of droughted and shaded plants (Table 2; Fig. 2, A) and up to 1.47 MPa between two

426 individuals. This is consistent with previous studies: Awad et al. (2010) reported a difference

427 of 0.63 MPa between droughted and well-watered plants; Plavcová and Hacke (2012) reported

428 a difference of 1.08 MPa between droughted and shaded *Populus trichocarpa x deltoides* plants.

429 Therefore, the plasticity induced by our experimental setup was probably close to the maximum

430 we could expect according to the literature.

431 The absence of difference in specific hydraulic conductivity (K_s) between droughted and control

432 plants (Table 2; Fig. 2, B) was consistent with the results of Gleason et al. (2016): who reported

433 a poor correlation between vulnerability to embolism and K_s in their meta-analysis.

434 Furthermore, the lack of trade-off between hydraulic efficiency and safety was also observed

435 within species (Awad et al. 2010, Plavcová and Hacke 2012, Schuldt et al. 2016). A significant

436 decrease of the theoretical conductivities (K_{s_theo}) was found for droughted plants compared to

437 other plants (Table 2), relying on a decrease in vessel diameter (D_v) (Table 3); whereas the pit

438 structure was not modified (Table 3). However, This theoretical decrease in lumen conductance

439 in droughted plants is only based on the Poiseuille's law and could be offset by other changes

440 we did not investigate, such as three-dimensional xylem organization, vessel wall sculpturing,

441 pit biochemistry or pit membrane porosity.

442 P_{50} was correlated with anatomical traits related to pit quantity characteristics measured at the

443 xylem and vessel levels (significant correlations with $R^2 > 0.7$ for 7 out of the 9 traits; Fig. 3,

444 4). These pit quantity parameters were correlated between them, which is not very surprising

445 since they all measure slightly different features of vessel connectivity (Table S2; Fig. S3).

446 Indeed, such correlations were also found when comparing *Acer* species (Lens et al. 2011). By

447 contrast, no correlation was found with the traits related to the pit dimensions (D_a, D_p, L_p and

448 T_m; Fig. 3). Thus, the pit ultrastructure does not appear as a driver of the plasticity of

449 vulnerability to embolism in *Populus tremula x alba* (Fig. S1). Despite a key role of T_m in

450 determining vulnerability to embolism, the air-seeding pressures for thin pit membrane such as

451 those of poplar xylem would not be influenced by slight changes in its thickness (Li et al. 2016,

452 Kaack et al. 2019). So, the role of pit structure in plasticity of vulnerability to embolism remains

453 to be tested in species having much thicker intervessel pit membranes. The observation of a

454 variation in vessel diameter not associated with a variation in pit membrane thickness is not

455 surprising, since this has already been reported when comparing the anatomy between organs

456 along the flow path in several species of angiosperm (Klepsch et al. 2018). Other relevant pit

457 parameters could also be considered, but suitable methods for investigating their variability are

458 lacking. For example, the pit membrane porosity contributes to the differences in vulnerability

459 to embolism (Jansen et al. 2009, Li et al. 2016, Kaack et al. 2019); but this parameter is difficult

460 to measure accurately because pores include a series of various pore constrictions, and the

461 narrowest constriction should be the main bottleneck (Kaack et al. 2019, Kaack et al. 2020,

462 Zhang et al. 2020). The role of the biochemical composition of the pit membrane in the

463 plasticity of vulnerability to embolism cannot be excluded too. Besides, there have been recent

464 advances in the understanding of the pit membrane biochemistry, including a role for lipids

465 (Herbette et al. 2015, Klepsch et al. 2016, Schenk et al. 2017, Pereira et al. 2018, Schenk et al.

466 2018, Kaack et al. 2019). Moreover, calcium in pit membrane was reported to be a major

467   determinant of between-species differences in vulnerability to embolism, but it was not

468   involved in the plasticity of vulnerability to embolism (Herbette and Cochard 2010).

469   At the interspecific level, pit ultrastructure parameters, especially the pit membrane thickness,

470   was identified as the major traits involved in variation in vulnerability to embolism (Jansen et

471   al. 2009; Tixier et al. 2014, Li et al. 2016, Kaack et al. 2019). In addition, between species

472   differences in vulnerability to embolism also depend on pit mechanical behaviour (Tixier et al.

473   2014). The probability for air seeding through large pores is expected to be higher when more

474   pits are present (rare pit hypothesis proposed by Christman et al. 2009). The pit area can thus

475   explain differences in vulnerability to embolism for some angiosperm groups but not for others

476   (Lens et al. 2013). Thus, when explaining the variability in vulnerability to embolism between

477   species, this trait, which depends on the vessel dimensions and xylem organization, does not

478   appear very relevant (Lens et al. 2013). Lens et al. (2011) tested the relationship between several

479   pit quantity and pit structure properties and vulnerability to embolism for 11 acer species. They

480   found that vulnerability to embolism strongly correlated with depth of bordered pit chamber

481   (L_p) and pit membrane thickness (T_m) whereas no relationship was found between vulnerability

482   to embolism and vessel diameter (D_v) and total pit area per vessel (A_p). By contrast, our results

483   suggest that the plasticity of vulnerability to embolism in poplar is controlled by the xylem

484   organization and vessel dimensions, and not by changes in pit structure. Thus, the mechanisms

485   controlling the inter-specific variability in vulnerability to embolism seem to be different from

486   the drivers of the within species plasticity in poplar. Complementary works on plasticity need

487   to be carried out on other species, particularly on species with much thicker pit membranes, in

488   order to test the genericity of the findings of this study. It would not be surprising if the

489   mechanisms of plasticity could be different depending on the species. A recent modelling

490   analysis of the relationships between the functional and structural pit properties provides some

491   interesting insights agreeing with our results and supporting different mechanisms for plasticity

492   (Kaack et al. 2020). According to this analysis considering the internal structure of the pit

493   membrane, three functional types of pit can be distinguished based on their T_m : (1) a pit with a

494   thin T_m (< 150 nm) would have large pores causing a low embolism resistance not very sensitive

495   to the pit area, (2) a pit with a thick T_m (>400 nm) with narrow pores allowing high embolism

496   resistance insensitive to the pit area and (3) an intermediate pit membrane type, with embolism

497   resistance strongly affected by the pit area. This latter type includes the case we studied and

498   thus it agrees well with our results. Indeed, the model predicts that the vulnerability to embolism

499   is strongly affected by the pit area for vessels with a pit membrane thickness of 250 nm.

500   The multispectral analysis combining X-ray microtomography analysis with light microscopy

501   revealed that P_e shows the strongest correlation with the position of the vessel relative to the

502   pith (Fig. 6). However, significant correlations were also found between the others xylem traits

503   (D_v, F_c and GS) and this radial position ($p < 0.001$), so no clear conclusion can be drawn about

504   an effect of vessel age or position on its vulnerability to embolism. The stem fully developed

505   in 3 months, and much less for the secondary xylem of the stem part investigated by X-ray

506   microtomography. We thus assume that the age difference is too weak to explain such

507   difference in vulnerability to embolism. Indeed, in diffuse-porous species, an age effect in

508   vulnerability to embolism has been reported between vessels formed in different years but not

509   between vessels of the same year (Melcher et al. 2003). Moreover, investigations of the

510   embolism spread in current-year stem of vine or walnut tree using the same approach did not

511   conclude to an age effect in the secondary xylem (Brodersen et al. 2013, Knipfer et al. 2015).

512   These two previous studies showed that embolisms formed first in vessels surrounding the pith,

513   then they spreaded overwhelmingly radially while the water potential was decreasing. The

514   sequence of embolism formation and spreading in our study could therefore be related to the

515   mechanism explained by Brodersen et al. (2013). More, we also hypothesize that vulnerability

516   to embolism decreased during development in relation to changing water conditions *in planta*.

517 Although the soil moisture content was kept constant, the midday water potential of the plant

518 decreased as the plant grew (Table 2). The pressure inducing embolism being correlated with

519 the midday water potential experienced by plants (Awad et al. 2010), the acclimation of

520 vulnerability to embolism would occur during the development of plants.

521 Vulnerability curves are commonly established by measuring the impact of embolism on the

522 conductance, but not the embolism rates. Thus, "hydraulic vulnerability" is a more suitable term

523 when comparing xylems for P_{50} using these methods. Conversely, X-ray microtomography

524 methods really allow assessing the local vulnerability to embolism.

525 Our results showing a strong relationship between P_{50} and some vessel and xylem tissue

526 parameters provide three non-exclusive explanations for the acclimation of hydraulic

527 vulnerability. This latter relies on changes in vulnerability to embolism of the vessels or on

528 changes in the effect of the embolism on conductance. First, our study shows that vulnerable

529 individuals exhibited larger vessels (both longer (L_v) and wider (D_v); Fig. 3). When a large

530 vessel embolizes, it generates a greater impact on the hydraulic conductivity compared to a

531 smaller vessel. Thus, a xylem having a high proportion of large vessels undergoes an important

532 drop of conductivity after each vessel embolism. Second, we found that vulnerable xylems had

533 a greater SI and a lower GI and F_c. Redundancy in the xylem has already been linked with a

534 lower hydraulic vulnerability using a modelling approach (Ewers et al. 2007, Mrad et al. 2018).

535 High connectivity and grouping is an efficient way to maintain the hydraulic conductance

536 despite embolized vessels in the xylem by providing alternative pathways to the water flow

537 (Carlquist 1966, Schuldt et al. 2016). Third, larger vessels have a larger pit area per vessel (A_p)

538 and would thus be more prone to embolism, according to the pit area hypothesis (Christman et

539 al. 2009). Multispectral analysis combining X-ray microtomography and light microscopy

540 allowed monitoring the dynamics of xylem embolism and in particular determining the

541 embolism pressure of each vessel (Fig.1; Fig. 5). This approach supports the third explanation,

542 since larger vessels (D_v^*) showed a higher vulnerability to embolism– as noticed by Cai and

543 Tyree (2010) using a statistical, indirect and destructive technique and by Jacobsen et al. (2019)

544 using a similar approach. Nevertheless, the poor correlations (low R^2 values) between the

545 embolism pressure of each vessel (P_e) and D_v^*, F_c^* or GS suggest that the rare pit hypothesis is

546 far from being sufficient for explaining the hydraulic vulnerability inside a stem sample.

547 According to Kaack et al. (2019), the rare pit hypothesis is not compatible with the three

548 dimensional structure of the pit. Other additional mechanisms could be involved to explain the

549 plasticity of hydraulic vulnerability observed among growth conditions: they would include the

550 effect of redundancy and of vessel embolized volume on the loss of conductance, or change in

551 pore constrictions in pit membranes. That is why we assume that the different mechanisms we

552 described here act together to design the hydraulic vulnerability during acclimation. The lowest

553 correlations found between P_e and F_c^* or GS point to the limitations of a bi-dimensional

554 approach to analyse vessel connectivity. Some studies reported analyses of the three-

555 dimensional xylem network (Brodersen et al. 2011), that allowed investigating events of

556 embolism formation and spreading (Brodersen et al. 2013, Knipfer et al. 2015, 2016, Torres et

557 al. 2016). Rather short segments (2-6 mm long) were examined what was enough for their study.

558 The vessels having an average length of about ten cm (up to 30 cm), would require analysis of

559 the vessel organization over a longer sample length for a full quantification of their

560 connectivity. This was impossible with the x-ray microtomograph device we used. Moreover,

561 such a large volume of wood could not be scanned without a very high temperature increase to

562 maintain sufficient resolution.

563 In conclusion, we found that the acclimation of vulnerability to embolism to contrasted growth

564 conditions in hybrid poplar did not rely on a change in pit ultrastructure, contrary to what was

565 reported when comparing species. Thus, within-species plasticity in hybrid poplar and between-

566 species variability for vulnerability to embolism could rely on different mechanisms. We

567 showed that an increase in resistance to embolism in poplar is related to an increase in vessels

568 connectivity and grouping and a decrease in vessel dimensions, leading to reduce the likelihood

569 of air seeding through a pit and the effect the resulting embolism events on hydraulic

570 conductance. This study will allow focusing on the relevant candidate genes controlling

571 vulnerability to embolism such as those involved in vessels grouping and connectivity or vessel

572 dimensions. These genes include the aquaporins involved in cell expansion during xylogenesis

573 (Plavcová et al. 2013), the genes controlling the cell wall metabolism in xylem such as *VND6*,

574 *VND7* and *MYB46*, which expression levels changed in response to an abiotic stress (Plavcová

575 et al. 2013, Taylor-Teeples et al. 2016) or *CLE* genes (*CLE41* and *CLE44*) that repress the

576 xylem differentiation (De Rybel et al. 2016).

577

587 **Authors' contributions**

588 C.L. and S.H. designed the study and wrote the manuscript with contributions from all authors.

589 C.L., S.H., P.C. and J.C. performed field work and hydraulic measurements; C.L., N.B-M.,

590 Y.Q., L.B. and J.S. performed electron microscopy; C.L., N.B-M., P.C. performed light

591   microscopy; C.L., P.C. and E.B. performed X-ray microCT; C.L., P.C. and E.B. performed

592   image analysis. All authors approved this manuscript.

References

Adams HD, Zeppel MJB, Anderegg WRL, Hartmann H, Landhäusser SM, Tissue DT, Huxman
        TE, Hudson PJ, Franz TE, Allen CD, Anderegg LDL, Barron-Gafford GA, Beerling DJ,
        Breshears DD, Brodribb TJ, Bugmann H, Cobb RC, Collins AD, Dickman LT, Duan H,
        Ewers BE, Galiano L, Galvez DA, Garcia-Forner N, Gaylord ML, Germino MJ, Gessler
        A, Hacke UG, Hakamada R, Hector A, Jenkins MW, Kane JM, Kolb TE, Law DJ, Lewis
        JD, Limousin J-M, Love DM, Macalady AK, Martínez-Vilalta J, Mencuccini M,
        Mitchell PJ, Muss JD, O'Brien MJ, O'Grady AP, Pangle RE, Pinkard EA, Piper FI,
        Plaut JA, Pockman WT, Quirk J, Reinhardt K, Ripullone F, Ryan MG, Sala A, Sevanto
        S, Sperry JS, Vargas R, Vennetier M, Way DA, Xu C, Yepez EA, McDowell NG (2017)
        A multi-species synthesis of physiological mechanisms in drought-induced tree
        mortality. Nat Ecol Evol 1:1285–1291.

Allario T, Tixier A, Awad H, Lemaire C, Brunel N, Badel É, Barigah TS, Julien J-L, Peyret P,
        Mellerowicz EJ, Cochard H, Herbette S (2018) PtxtPME1 and homogalacturonans
        influence xylem hydraulic properties in poplar. Physiol Plant 163:502–515.

Anderegg WRL, Flint A, Huang C, Flint L, Berry JA, Davis FW, Sperry JS, Field CB (2015)
        Tree mortality predicted from drought-induced vascular damage. Nature Geosci 8:367–
        371.

Anderegg WRL, Klein T, Bartlett M, Sack L, Pellegrini AFA, Choat B, Jansen S (2016) Meta-
        analysis reveals that hydraulic traits explain cross-species patterns of drought-induced
        tree mortality across the globe. PNAS 113:5024–5029.

Awad H, Barigah T, Badel É, Cochard H, Herbette S (2010) Poplar vulnerability to xylem
        cavitation acclimates to drier soil conditions. Physiol Plant 139:280–288.

Barigah TS, Charrier O, Douris M, Bonhomme M, Herbette S, Améglio T, Fichot R, Brignolas
        F, Cochard H (2013) Water stress-induced xylem hydraulic failure is a causal factor of
        tree mortality in beech and poplar. Ann Bot 112:1431–1437.

Barigah TS, Ibrahim T, Bogard A, Faivre-Vuillin B, Lagneau LA, Montpied P, Dreyer E (2006)
        Irradiance-induced plasticity in the hydraulic properties of saplings of different
        temperate broad-leaved forest tree species. Tree Physiol 26:1505–1516.

Brodersen CR, Lee EF, Choat B, Jansen S, Phillips RJ, Shackel KA, McElrone AJ, Matthews
        MA (2011) Automated analysis of three-dimensional xylem networks using high-
        resolution computed tomography. New Phytol 191(4), 1168-1179.

Brodersen CR, McElrone AJ, Choat B, Lee EF, Shackel KA, Matthews MA (2013) In vivo
        visualizations of drought-induced embolism spread in *Vitis vinifera*. Plant Physiol
        161(4): 1820-1829.

Cai J, Tyree MT (2010) The impact of vessel size on vulnerability curves: data and models for
        within-species variability in saplings of aspen, Populus tremuloides Michx. Plant Cell
        Env 33:1059–1069.

Carlquist S (1966) Wood Anatomy of Compositae: A Summary, With Comments on Factors
        Controlling Wood Evolution. Aliso: A Journal of Systematic and Evolutionary Botany
        6:25–44.

634 Choat B, Cobb AR, Jansen S (2008) Structure and function of bordered pits: new discoveries
635   and impacts on whole-plant hydraulic function. New Phytol 177: 608–626.

636 Choat B, Jansen S, Brodribb TJ, Cochard H, Delzon S, Bhaskar R, Bucci SJ, Feild TS, Gleason
637   SM, Hacke UG, Jacobsen AL, Lens F, Maherali H, Martínez-Vilalta J, Mayr S,
638   Mencuccini M, Mitchell PJ, Nardini A, Pittermann J, Pratt RB, Sperry JS, Westoby M,
639   Wright IJ, Zanne AE (2012) Global convergence in the vulnerability of forests to
640   drought. Nature 491:752–755.

641 Choat B, Pittermann J (2009) New insights into bordered pit structure and cavitation resistance
642   in angiosperms and conifers. New Phytol 182: 557-560.

643 Christman MA, Sperry JS, Adler FR (2009) Testing the 'rare pit' hypothesis for xylem
644   cavitation resistance in three species of Acer. New Phytol 182:664–674.

645 Cochard H (2002) A technique for measuring xylem hydraulic conductance under high negative
646   pressures. Plant Cell Env 25:815–819.

647 Cochard H, Badel E, Herbette S, Delzon S, Choat B, Jansen S (2013) Methods for measuring
648   plant vulnerability to cavitation: a critical review. J Exp Bot 64:4779–4791.

649 Cochard H, Damour G, Bodet C, Tharwat I, Poirier M, Améglio T (2005) Evaluation of a new
650   centrifuge technique for rapid generation of xylem vulnerability curves. Physiol Plant
651   124:410–418.

652 Cochard H, Delzon S, Badel É (2015) X-ray microtomography (micro-CT): a reference
653   technology for high-resolution quantification of xylem embolism in trees. Plant Cell
654   Env 38:201–206.

655 Cochard H, Hölttä T, Herbette S, Delzon S, Mencuccini M (2009) New insights into the
656   mechanisms of water-stress-induced cavitation in conifers. Plant Physiol 151:949–954.

657 Cohen S, Bennink J, Tyree M (2003) Air method measurements of apple vessel length
658   distributions with improved apparatus and theory. J Exp Bot 54:1889–1897.

659 Cooke JEK, Martin TA, Davis JM (2005) Short-term physiological and developmental
660   responses to nitrogen availability in hybrid poplar. New Phytol 167:41–52.

661 De Rybel B, Mähönen AP, Helariutta Y, Weijers D (2016) Plant vascular development: from
662   early specification to differentiation. Nat Rev Mol Cell Biol 17:30–40.

663 Domec J-C, Gartner BL (2001) Cavitation and water storage capacity in bole xylem segments
664   of mature and young Douglas-fir trees. Trees 15:204–214.

665 Ewers FW, Ewers JM, Jacobsen AL, López-Portillo J (2007) Vessel redundancy: Modeling
666   safety in numbers. IAWA J 28:373–388.

667 Fichot R, Barigah TS, Chamaillard S, Le Thiec D, Laurans F, Cochard H, Brignolas F (2010)
668   Common trade-offs between xylem resistance to cavitation and other physiological
669   traits do not hold among unrelated Populus deltoides ×Populus nigra hybrids. Plant Cell
670   Env 33:1553–1568.

Gleason SM, Westoby M, Jansen S, Choat B, Hacke UG, Pratt RB, Bhaskar R, Brodribb TJ, Bucci SJ, Cao K-F, Cochard H, Delzon S, Domec J-C, Fan Z-X, Feild TS, Jacobsen AL, Johnson DM, Lens F, Maherali H, Martínez-Vilalta J, Mayr S, McCulloh KA, Mencuccini M, Mitchell PJ, Morris H, Nardini A, Pittermann J, Plavcová L, Schreiber SG, Sperry JS, Wright IJ, Zanne AE (2016) Weak tradeoff between xylem safety and xylem-specific hydraulic efficiency across the world's woody plant species. New Phytol 209:123–136.

Hacke UG, Sperry JS, Wheeler JK, Castro L (2006) Scaling of angiosperm xylem structure with safety and efficiency. Tree Physiol 26: 689–701.

Hajek P, Leuschner C, Hertel D, Delzon S, Schuldt B (2014) Trade-offs between xylem hydraulic properties, wood anatomy and yield in *Populus*. Tree Physiol 34:744–756.

Hammond WM, Yu K, Wilson LA, Will RE, Anderegg WRL, Adams HD (2019) Dead or dying? Quantifying the point of no return from hydraulic failure in drought-induced tree mortality. New Phytol 223:1834–1843.

Hartmann H, McDowell NG, Trumbore S (2015) Allocation to carbon storage pools in Norway spruce saplings under drought and low CO2. Tree Physiol 35:243–252.

Herbette S, Bouchet B, Brunel N, Bonnin E, Cochard H, Guillon F (2015) Immunolabelling of intervessel pits for polysaccharides and lignin helps in understanding their hydraulic properties in Populus tremula × alba. Ann Bot 115:187–199.

Herbette S, Cochard H (2010) Calcium Is a Major Determinant of Xylem Vulnerability to Cavitation. Plant Physiol 153:1932–1939.

Herbette S, Wortemann R, Awad H, Huc R, Cochard H, Barigah TS (2010) Insights into xylem vulnerability to cavitation in Fagus sylvatica L.: phenotypic and environmental sources of variability. Tree Physiol 30:1448–1455.

Jacobsen AL, Pratt RB, Venturas MD, Hacke UG (2019) Large volume vessels are vulnerable to water-stress-induced embolism in stems of poplar. IAWA J 40: 4-22.

Jansen S, Klepsch M, Li S, Kotowska M, Schiele S, Zhang Y, Schenk H (2018) Challenges in understanding air-seeding in angiosperm xylem. Acta Hort 1222: 13-20.

Jansen S, Choat B, Pletsers A (2009) Morphological variation of intervessel pit membranes and implications to xylem function in angiosperms. Am J Bot 96:409–419.

Jinagool W, Lamacque L, Delmas M, Delzon S, Cochard H, Herbette S (2018) Is there variability for xylem vulnerability to cavitation in walnut tree cultivars and species (Juglans spp.)? HortSci 53:132–137.

Jinagool W, Rattanawong R, Sangsing K, Barigah TS, Gay F, Cochard H, Kasemsap P, Herbette S (2015) Clonal variability for vulnerability to cavitation and other drought-related traits in Hevea brasiliensis Müll. Arg. J Plant Hydraul 2:e001.

Kaack L, Altaner CM, Carmesin C, Diaz A, Holler M, Kranz C, Neusser G, Odstrcil M, Schenk HJ, Schmidt V, Weber M, Zhang Y, Jansen S (2019) Function and three-dimensional structure of intervessel pit membranes in angiosperms: a review. IAWA J 40:673–702.

710   Kaack L, Weber M, Isasa E, Karimi Z, Li S, Pereira L, Trabi CL, Zhang Y, Schenk HJ, Schuldt
711   B, Schmidt V, Jansen S (2020) Pore constrictions in intervessel pit membranes reduce
712   the risk of embolism spreading in angiosperm xylem. bioRxiv:345413.

713   Klepsch MM, Schmitt M, Paul Knox J, Jansen S (2016) The chemical identity of intervessel pit
714   membranes in Acer challenges hydrogel control of xylem hydraulic conductivity. AoB
715   PLANTS 8: plw052.

716   Klepsch M, Zhang Y, Kotowska MM, Lamarque LJ, Nolf M, Schuldt B, Torres-Ruiz JM, Qin
717   D-W, Choat B, Delzon S, Scoffoni C, Cao K-F, Jansen S (2018) Is xylem of angiosperm
718   leaves less resistant to embolism than branches? Insights from microCT, hydraulics, and
719   anatomy. J Exp Bot 69:5611–5623.

720   Knipfer T, Brodersen CR, Zedan A, Kluepfel DA, McElrone AJ (2015) Patterns of drought-
721   induced embolism formation and spread in living walnut saplings visualized using X-
722   ray microtomography. Tree Physiol 35: 744-755.

723   Knipfer T, Cuneo IF, Brodersen CR, McElrone AJ (2016) In situ visualization of the dynamics
724   in xylem embolism formation and removal in the absence of root pressure: a study on
725   excised grapevine stems. Plant Physiol 171(2), 1024-1036.

726   Lamy J-B, Bouffier L, Burlett R, Plomion C, Cochard H, Delzon S (2011) Uniform selection
727   as a primary force reducing population genetic differentiation of cavitation resistance
728   across a species range. PLOS ONE 6:e23476.

729   Lamy J-B, Plomion C, Kremer A, Delzon S (2012) QST < FST As a signature of canalization.
730   Mol Ecol 21:5646–5655.

731   Lens F, Sperry JS, Christman MA, Choat B, Rabaey D, Jansen S (2011) Testing hypotheses
732   that link wood anatomy to cavitation resistance and hydraulic conductivity in the genus
733   Acer. New Phytol 190:709–723.

734   Lens F, Tixier A, Cochard H, Sperry JS, Jansen S, Herbette S (2013) Embolism resistance as a
735   key mechanism to understand adaptive plant strategies. Cur Op Plant Biol 16:287–292.

736   Li S, Lens F, Espino S, Karimi Z, Klepsch M, Schenk HJ, Schmitt M, Schuldt B, Jansen S
737   (2016) Intervessel pit membrane thickness as a key determinant of embolism resistance
738   in angiosperm xylem. IAWA J 37:152–171.

739   Loepfe L, Martinez-Vilalta J, Pinol J, Mencuccini M (2017) The relevance of the xylem
740   network structure for plant hydraulic efficiency and safety. J Th Biol 247: 788-803.

741   Maherali H, Moura CF, Caldeira MC, Willson CJ, Jackson RB (2006) Functional coordination
742   between leaf gas exchange and vulnerability to xylem cavitation in temperate forest
743   trees. Plant Cell Env 29:571–583.

744   Martínez-Vilalta J, Cochard H, Mencuccini M, Sterck F, Herrero A, Korhonen JFJ, Llorens P,
745   Nikinmaa E, Nolè A, Poyatos R, Ripullone F, Sass-Klaassen U, Zweifel R (2009)
746   Hydraulic adjustment of Scots pine across Europe. New Phytol 184:353–364.

747   Melcher PJ, Zwieniecki MA, Holbrook NM (2003) Vulnerability of xylem vessels to cavitation
748   in sugar maple. Scaling from individual vessels to whole branches. Plant Physiol 131(4):

749   1775-1780.

750   Mrad A, Domec JC, Huang CW, Lens F, Katul G (2018) A network model links wood anatomy
751   to xylem tissue hydraulic behaviour and vulnerability to cavitation. Plant Cell Env
752   41:2718-2730.

753   Niez B, Dlouha J, Moulia B, Badel É (2019) Water-stressed or not, the mechanical acclimation
754   is a priority requirement for trees. Trees 33:279–291.

755   Pammenter NW, Van der Willigen C (1998) A mathematical and statistical analysis of the
756   curves illustrating vulnerability of xylem to cavitation. Tree Physiol 18:589–593.

757   Pereira L, Flores-Borges DNA, Bittencourt PRL, Mayer JLS, Kiyota E, Araújo P, Jansen S,
758   Freitas RO, Oliveira RS, Mazzafera P (2018) Infrared nanospectroscopy reveals the
759   chemical nature of pit membranes in water-conducting cells of the plant xylem. Plant
760   Physiol 177:1629–1638.

761   Plavcová L, Hacke UG (2012) Phenotypic and developmental plasticity of xylem in hybrid
762   poplar saplings subjected to experimental drought, nitrogen fertilization, and shading. J
763   Exp Bot 63:6481–6491.

764   Plavcová L, Hacke UG, Sperry JS (2011) Linking irradiance-induced changes in pit membrane
765   ultrastructure with xylem vulnerability to cavitation. Plant Cell Env 34:501–513.

766   Plavcová L, Jansen S, Klepsch M, Hacke UG (2013) Nobody's perfect: can irregularities in pit
767   structure influence vulnerability to cavitation? Front Plant Sci 4: 453.

768   Schenk HJ, Espino S, Romo DM, Nima N, Do AYT, Michaud JM, Papahadjopoulos-Sternberg
769   B, Yang J, Zuo YY, Steppe K, Jansen S (2017) Xylem surfactants introduce a new
770   element to the cohesion-tension theory. Plant Physiol 173:1177–1196.

771   Schenk, H. J., Espino, S., Rich-Cavazos, S. M., & Jansen, S. (2018). From the sap's perspective:
772   the nature of vessel surfaces in angiosperm xylem. Am J Bot 105:174-187.

773   Schindelin J, Arganda-Carreras I, Frise E, Kaynig V, Longair M, Pietzsch T, Preibisch S,
774   Rueden C, Saalfeld S, Schmid B, Tinevez J-Y, White DJ, Hartenstein V, Eliceiri K,
775   Tomancak P, Cardona A (2012) Fiji: an open-source platform for biological-image
776   analysis. Nature Methods 9:676–682.

777   Schneider CA, Rasband WS, Eliceiri KW (2012) NIH Image to ImageJ: 25 years of image
778   analysis. Nature Methods 9:671–675.

779   Scholander PF, Bradstreet ED, Hemmingsen EA, Hammel HT (1965) Sap pressure in vascular
780   plants: Negative hydrostatic pressure can be measured in plants. Sci 148:339–346.

781   Scholz A, Klepsch M, Karimi Z, Jansen S (2013b) How to quantify conduits in wood? Front
782   Plant Sci 4:56.

783   Scholz A, Rabaey D, Stein A, Cochard H, Smets E, Jansen S (2013a) The evolution and function
784   of vessel and pit characters with respect to cavitation resistance across 10 Prunus
785   species. Tree Physiol 33:684–694.

786   Schuldt B, Knutzen F, Delzon S, Jansen S, Müller-Haubold H, Burlett R, Clough Y, Leuschner
787   C (2016) How adaptable is the hydraulic system of European beech in the face of climate
788   change-related precipitation reduction? New Phytol 210:443–458.

789   Sperry JS, Hacke UG, Wheeler JK (2005) Comparative analysis of end wall resistivity in xylem
790   conduits. Plant Cell Env 28:456–465.

791   Steudle E (2001) The cohesion-tension mechanism and the acquisition of water by plant roots.
792   Ann Rev Plant Physiol Plant Molecul Biol 52:847–875.

793   Taylor-Teeples M, Lin L, Lucas M de, Turco G, Toal TW, Gaudinier A, Young NF, Trabucco
794   GM, Veling MT, Lamothe R, Handakumbura PP, Xiong G, Wang C, Corwin J,
795   Tsoukalas A, Zhang L, Ware D, Pauly M, Kliebenstein DJ, Dehesh K, Tagkopoulos I,
796   Breton G, Pruneda-Paz JL, Ahnert SE, Kay SA, Hazen SP, Brady SM (2015) An
797   Arabidopsis gene regulatory network for secondary cell wall synthesis. Nature 517:571–
798   575.

799   Tixier A, Herbette S, Jansen S, Capron M, Tordjeman P, Cochard H, Badel É (2014) Modelling
800   the mechanical behaviour of pit membranes in bordered pits with respect to cavitation
801   resistance in angiosperms. Ann Bot 114:325–334.

802   Torres-Ruiz J.M., Cochard H., Mencuccini M., Delzon S., Badel E. 2016. Direct observations
803   and modelling of embolism spread between xylem conduits: a case study in Scot pine.
804   Plant Cell Env 39:2774-2785.

805   Tyree MT, Davis SD, Cochard H (1994) Biophysical perspectives of xylem evolution: is there
806   a tradeoff of hydraulic efficiency for vulnerability to dysfunction? IAWA J 15:335–360.

807   Wheeler JK, Sperry JS, Hacke UG, Hoang N (2005) Inter-vessel pitting and cavitation in woody
808   Rosaceae and other vesselled plants: a basis for a safety versus efficiency trade-off in
809   xylem transport. Plant Cell Env 28:800–812.

810   Wortemann R, Herbette S, Barigah TS, Fumanal B, Alia R, Ducousso A, Gomory D, Roeckel-
811   Drevet P, Cochard H (2011) Genotypic variability and phenotypic plasticity of
812   cavitation resistance in Fagus sylvatica L. across Europe. Tree Physiol 31:1175–1182.

813   Zimmermann MH, Jeje AA (1981) Vessel-length distribution in stems of some American
814   woody plants. Can J Bot 59:1882–1892.

815   Zhang Y, Carmesin C, Kaack L, Klepsch MM, Kotowska M, Matei T, Schenk HJ, Weber M,
816   Walther P, Schmidt V, Jansen S (2020) High porosity with tiny pore constrictions and
817   unbending pathways characterize the 3D structure of intervessel pit membranes in
818   angiosperm xylem. Plant Cell Env 43:116–130.

819   Figure 1: Measurement of the embolism pressure (P_e) of each individual vessel. A-D: Direct

820   observation of embolism spread using a x-ray microtomograph in an intact xylem stem under

821   increasing tension. Black areas reveal the embolized vessels. A: native state ($\Psi = 0$ MPa).

822   B: $\Psi = -1.5$ MPa. C: P_{50} state ($\Psi = -2.5$ MPa). D: final state ($\Psi = -4$ MPa). E: Cut of the same

823   stem sample observed using light microscopy. The resulting image resolution allows us

824   measuring accurately the anatomical traits. Colour represents the embolism pressure (P_e) of

825   each vessel, as measured with x-ray microtomography. Shown images are from a subset of

826   approx. 230 vessels on a control plant.

827

828   Figure 2: Xylem hydraulic traits in trees depending on the growth conditions. A: Xylem

829   vulnerability curve. Each line is the mean curve per condition: droughted, n = 9 from 9 trees;

830   control, n = 10 from 5 trees; shaded, n = 12 from 6 trees. Dashed line, droughted plants; full

831   line, control plants; dotted line, shaded plants. Grey areas represent the standard deviations

832   around the means. Horizontal dotted line indicates the 50 % loss of conductance. B: Hydraulic

833   specific conductivity (K_s). Data are mean values for 8 droughted trees, 9 control trees, 9 shaded

834   trees. Error bars show the standard deviation.

835

836   Figure 3: Correlation between P_{50} and several xylem structural traits. Data are squares of the

837   coefficient of correlation (R^2) for each factor with P_{50}. Black bars indicate pit-related traits and

838   white bars indicate vessel and xylem-related traits. On the x-axis, a "+" symbol indicates a

839   positive correlation, while a "-" symbol indicates a negative one. Stars indicate the significance

840   of the correlation: "***", $p < 0.001$; "**", $0.001 < p < 0.01$; "ns", non-significant correlation.

841

842   Figure 4: Correlation between P_{50} and two xylem structural traits. A: Relationship between P_{50}

843   and pit area per vessel (A_p). B: Relationship between P_{50} and vessel grouping index (GI). Each

844   point represents the mean value for an individual tree. Black circles refer to droughted plants;

845   white circles refer to control plants and white squares refer to shaded plants. The dotted line is

846   the regression line.

847

848   Figure 5: Correlation between P_e and vessel traits within xylem. Data are all vessel

849   measurements pooled from analyses on four individuals using X-ray microtomography. A-C:

850   Vulnerability to embolism curves of vessels grouped by classes depending on structural traits.

851   A: Vessels clustered by diameter (D_v^*) classes. The dash sizes of the lines indicate the vessel

852   diameter class: from full line (narrow vessels) to dotted line (wide vessels). B: Vessels clustered

853   by classes for fraction of membrane length in contact with other vessels (F_c^*). The dash sizes

854   of the lines indicate the vessel contact fraction class: from full line (non-contact vessels) to

855   dotted line (vessels sharing high portion of membrane length). C: Vessels are clustered by group

856   size (GS) classes. The dash sizes of the lines indicate the vessel group sizes: from full line

857   (solitary vessels) to dotted line (vessels in large groups). D: Vessels clustered by distance from

858   the pith. The relative distance is between 0 and 1, 0 being close to the pith. The dash sizes of

859   the lines indicate the vessel distance class: from full line (vessels close to the pith) to dotted line

860   (vessels far from the pith).

861   Figure 6: Correlation between P_e and xylem traits. Data are squares of the coefficient of

862   correlation (R^2) for each factor with P_e. On the x-axis, a "+" symbol indicates a positive

863   correlation, while a "-" symbol indicates a negative one. Stars indicate the significance of the

864   correlation for the trait: "***", $p < 0.001$.

Table 1: Meanings of the symbols.

Symbol	Definition	Unit
Ψ_{pd}	Predawn water potential	MPa
Ψ_{md}	Midday water potential	MPa
LA	Mean leaf area	cm²
A_p	Mean total pit area per vessel	mm²
A_v	Mean area per vessel	mm²
D_a	Mean pit aperture diameter	μm
D_p	Mean pit diameter	μm
D_v	Mean vessel diameter	μm
D_v^*	Vessel diameter	μm
F_c	Mean contact fraction: mean membrane length in contact with other vessels over total membrane length	%
F_c^*	Vessel contact fraction: for each vessel, fraction of membrane length in contact with other vessels	%
F_p	Mean pit fraction: mean total pit area in contact with other vessels over total vessel area	%
F_{pf}	Mean pit-field fraction: pit area over inter-vessel area	%
GI	Vessel grouping index	-
GS	Vessel group size	-
K_{s_theo}	Theoretical hydraulic conductivity	kg.s^{-1}.MPa^{-1}.m^{-1}
K_s	Specific hydraulic conductivity	kg.s^{-1}.MPa^{-1}.m^{-1}
L_p	Mean pit chamber depth	μm
L_v	Median vessel length	μm
P_{50}, P_{12}, P_{88}	Pressure inducing 50, 12, 88 % loss of xylem conductance	MPa
P_e	Pressure inducing embolism in a vessel	MPa
SI	Vessel solitary index	%
T_m	Mean pit membrane thickness	μm

Table 2: Physiological characterisation of sapling grown under the three different conditions.

Factor	Unit	Droughted	Control	Shaded
Ψ_{pd} m-1	Mpa	- 0.22 ± 0.12 [a]	- 0.11 ± 0.04 [b]	- 0.13 ± 0.01 [b]
Ψ_{md} m-1	MPa	- 0.96 ± 0.15 [a]	- 0.69 ± 0.05 [b]	- 0.77 ± 0.09 [b]
Ψ_{pd} d-1	Mpa	- 0.59 ± 0.44 [a]	- 0.14 ± 0.03 [b]	- 0.11 ± 0.02 [b]
Ψ_{md} d-1	MPa	- 1.44 ± 0.33 [a]	- 0.98 ± 0.06 [b]	- 0.98 ± 0.11 [b]
LA	cm²	87.64 ± 18.41 [a]	137.61 ± 17.55 [b]	184.13 ± 40.34 [c]
Height	Mm	1685 ± 187 [a]	2237 ± 263 [b]	2282 ± 76 [b]
Diameter	Mm	9.47 ± 0.83 [a]	13.96 ± 0.49 [b]	10.94 ± 0.61 [b]
K_{s_theo}	kg.s^{-1}.MPa^{-1}.m^{-1}	0.949 ± 0.336 [a]	1.380 ± 0.274 [b]	1.405 ± 0.198 [b]
K_s	kg.s^{-1}.MPa^{-1}.m^{-1}	1.054 ± 0.192 [a]	1.043 ± 0.301 [a]	0.954 ± 0.330 [a]
P_{50}	MPa	- 3.03 ± 0.23 [a]	- 2.49 ± 0.10 [b]	- 2.27 ± 0.18 [b]
P_{12}	MPa	- 2.55 ± 0.34 [a]	- 2.02 ± 0.11 [b]	- 1.87 ± 0.11 [b]
P_{88}	MPa	- 3.51 ± 0.24 [a]	- 2.95 ± 0.11 [b]	- 2.68 ± 0.11 [b]
Native Embolism	%	1.81 ± 10.47 [a]	- 7.48 ± 7.91 [ab]	- 10.81 ± 7.84 [b]

Data are mean values ± standard deviation for each growth condition. For each line, values not followed by the same letter differ significantly at $p < 0.05$ (one-way ANOVA). Water potentials (Ψ_{pd} and Ψ_{md}) were measured one month before (m-1) and the day before (d-1) stem sampling for hydraulic and structural analysis. Ψ_{pd}, Predawn water potential; Ψ_{md}, Midday water potential; LA, Leaf area; K_{s_theo}, Theoretical hydraulic conductivity; K_s, Specific hydraulic conductivity; P_{50}; P_{12}; P_{88}, pressure inducing 50; 12 and 88 percent loss of conductance.

Table 3: Xylem structural traits depending on the growth conditions.

Trait	Unit	Droughted	Control	Shaded
A_p	mm^2	1.20 ± 0.51^a	2.94 ± 0.65^b	3.78 ± 0.27^c
A_v	mm^2	8.21 ± 3.93^a	20.63 ± 3.64^b	26.65 ± 8.22^b
D_a	μm	3.67 ± 0.34	3.37 ± 0.61	3.98 ± 0.81
D_p	μm	9.18 ± 0.69	8.64 ± 0.55	8.89 ± 0.72
D_v	μm	31.22 ± 6.14^a	40.07 ± 1.98^b	42.71 ± 2.28^b
F_c	%	20.35 ± 2.70^a	19.01 ± 1.13^b	17.04 ± 0.96^c
F_p	%	15.95 ± 1.13^a	14.15 ± 0.77^b	12.53 ± 0.56^c
F_{pf}	%	74.45 ± 1.33	74.46 ± 2.93	74.13 ± 2.75
GI	-	1.84 ± 0.20^a	1.63 ± 0.05^b	1.51 ± 0.05^c
L_p	μm	1.99 ± 0.06	2.08 ± 0.03	1.87 ± 0.11
L_v	mm	70.79 ± 25.1^a	137.0 ± 18.86^b	164.6 ± 48.4^c
SI	%	33.13 ± 5.43^a	38.46 ± 2.19^b	43.73 ± 3.11^c
T_m	μm	0.26 ± 0.04	0.23 ± 0.04	0.24 ± 0.02

The meaning of the symbols is given in Table 1. For each trait, the method for measurement and number of replication are indicated in the methods section. Data are mean values ± standard deviation. For each line, values not followed by the same letter differ significantly at *p < 0.05* (one-way ANOVA).
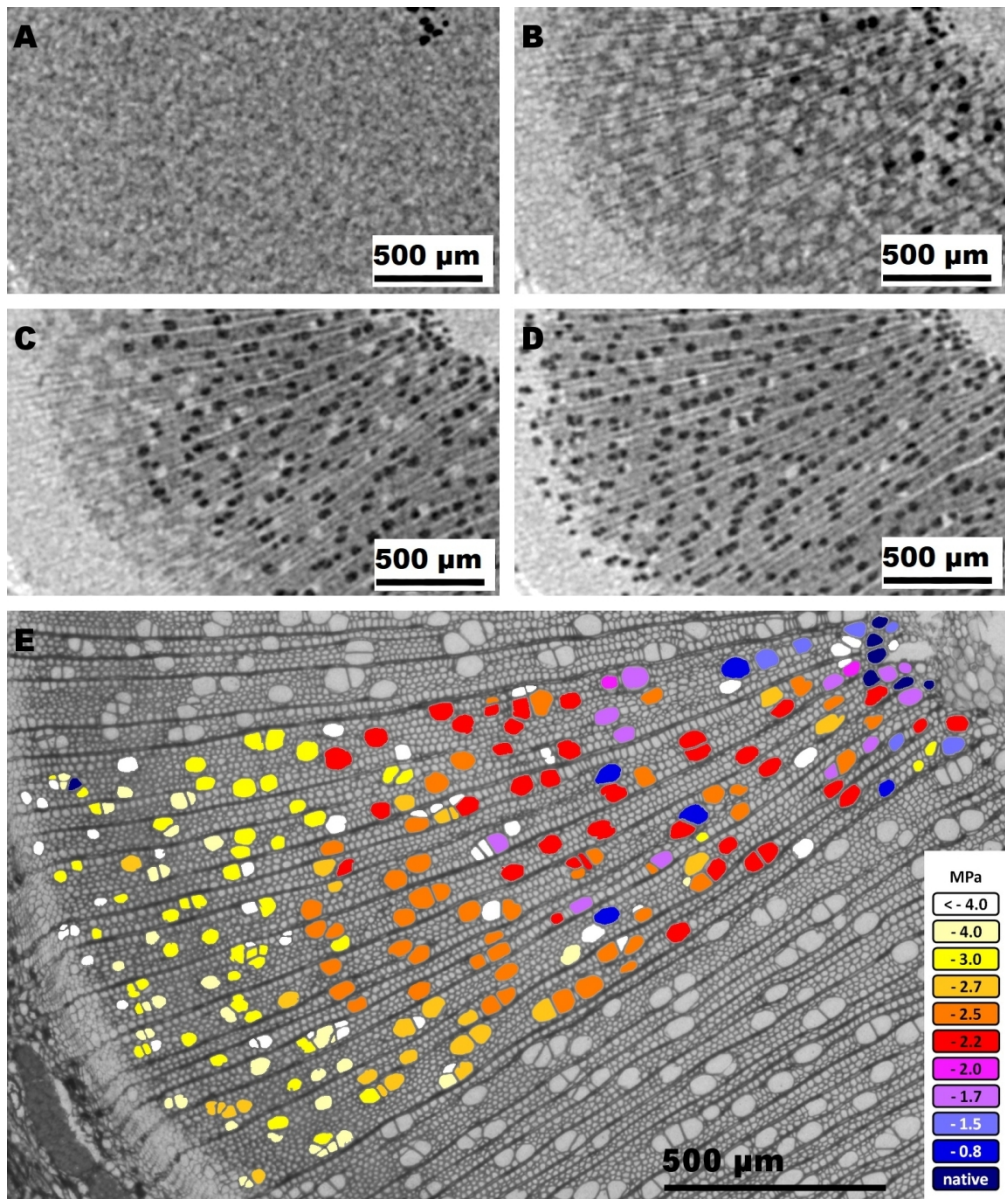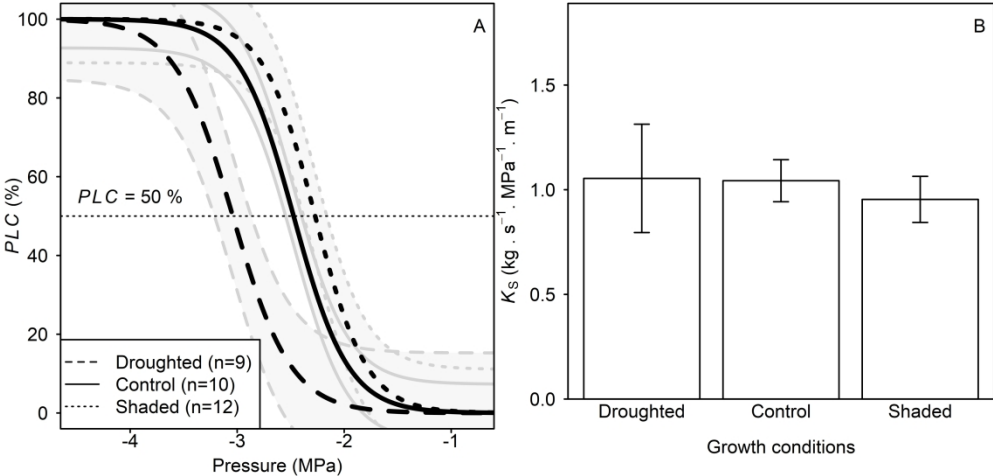
figure 1

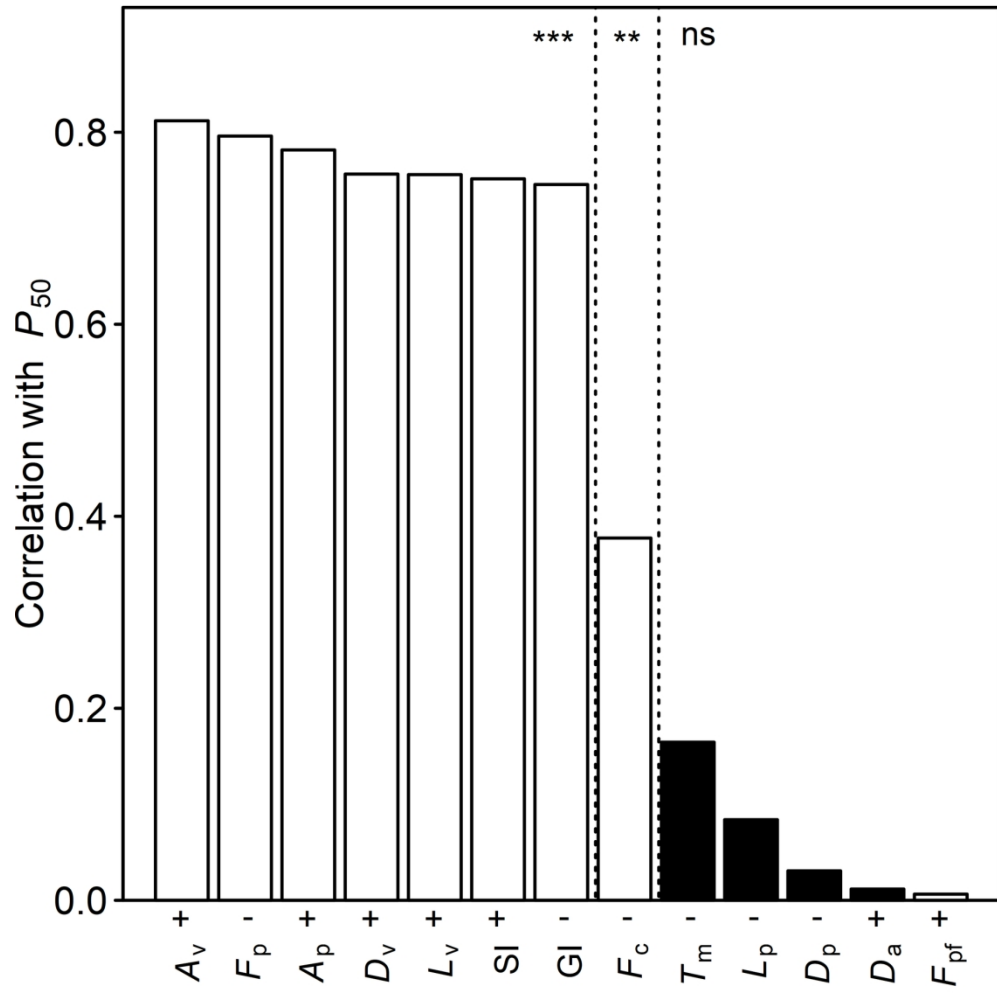339x404mm (120 x 120 DPI)

figure 2

171x82mm (600 x 600 DPI)

figure 3
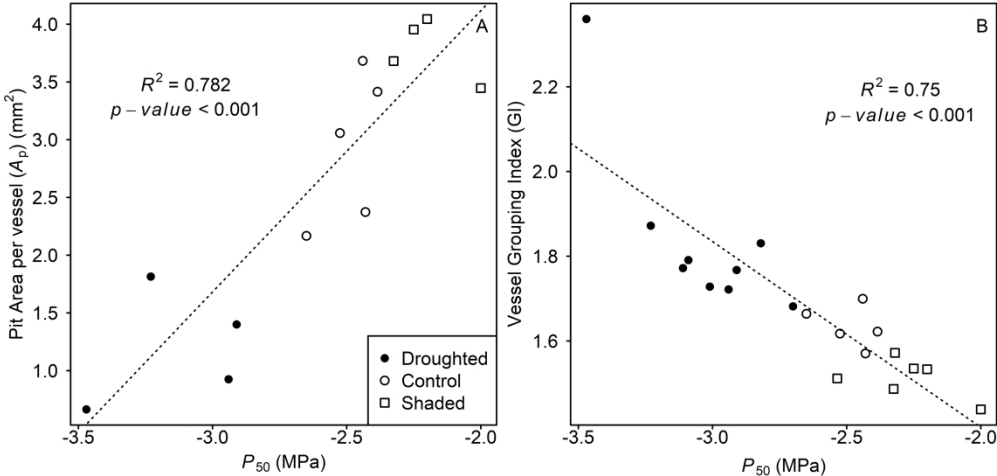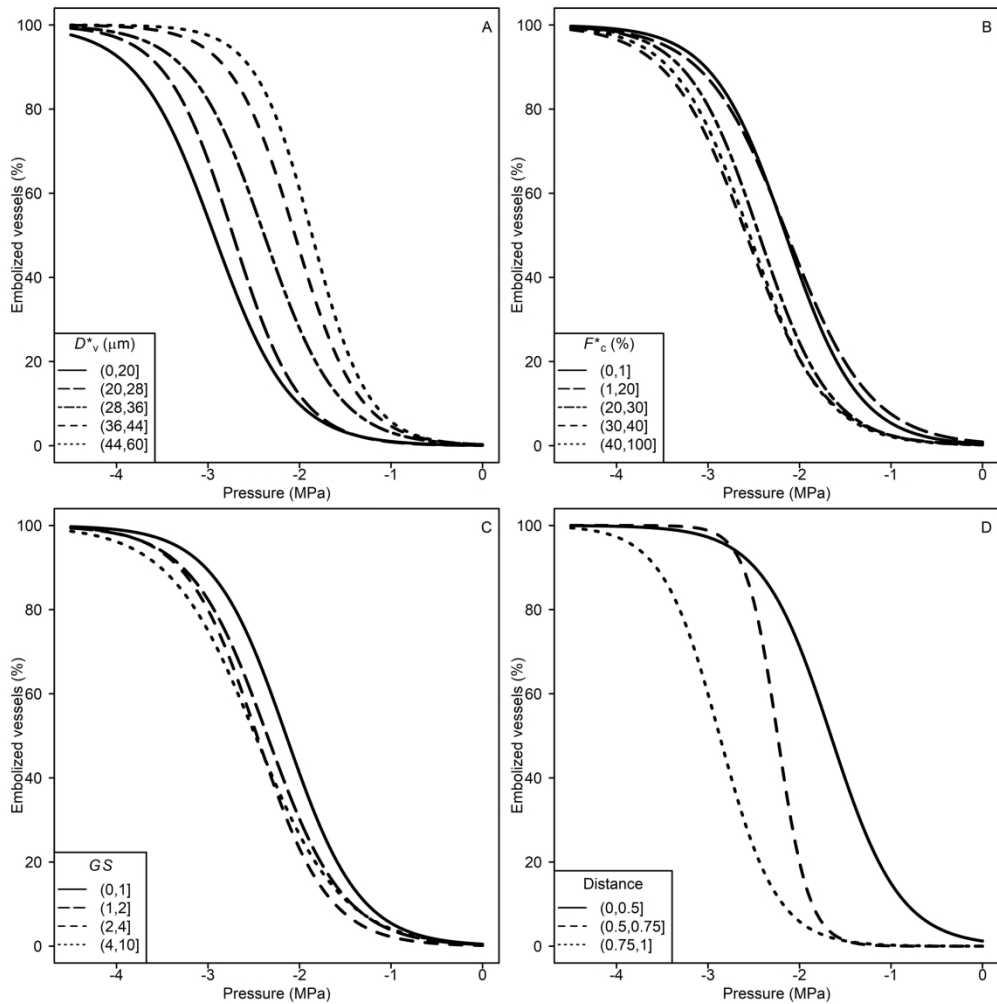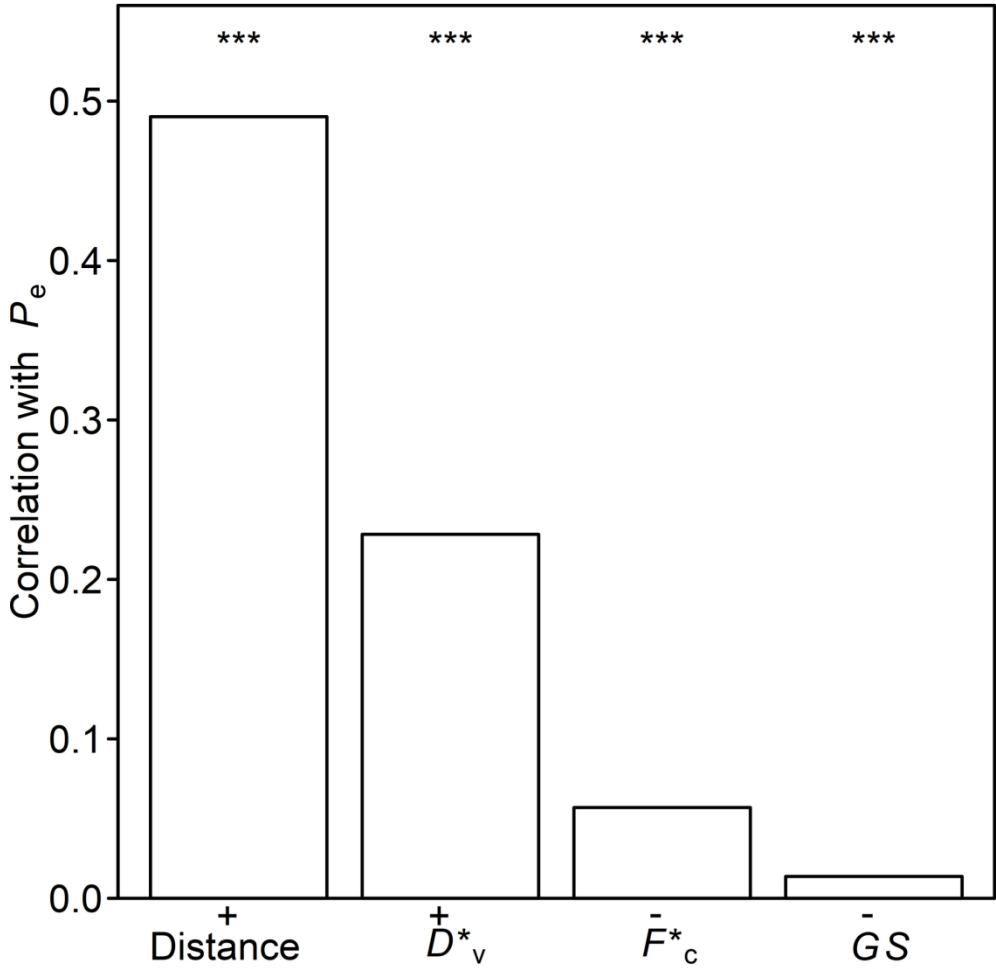
82x82mm (600 x 600 DPI)

figure 4

171x82mm (600 x 600 DPI)

figure5

114x114mm (600 x 600 DPI)

figure 6

82x82mm (600 x 600 DPI)